IEEE Photonics Journal
An IEEE Photonics Society Publication

Open Access

# Predictions of Free-Carrier Electroabsorption and Electrorefraction in Germanium

Volume 7, Number 3, June 2015

**Milos Nedeljkovic**
**Richard Soref**
**Goran Z. Mashanovich**

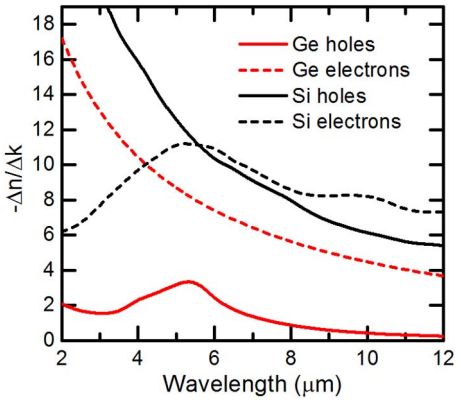


DOI: 10.1109/JPHOT.2015.2419217
1943-0655 © 2015 IEEE

IEEE photonics SOCIETY

IEEE

# Predictions of Free-Carrier Electroabsorption and Electrorefraction in Germanium

**Milos Nedeljkovic,[1] Richard Soref,[2] and Goran Z. Mashanovich[1]**

[1]Optoelectronics Research Centre, University of Southampton, Southampton SO17 1BJ, U.K.
[2]Physics and Engineering Departments, University of Massachusetts at Boston, Boston, MA 02125 USA

*DOI: 10.1109/JPHOT.2015.2419217*
*This work is licensed under a Creative Commons Attribution 3.0 License.*
*For more information, see http://creativecommons.org/licenses/by/3.0/*

Manuscript received March 10, 2015; accepted March 31, 2015. Date of current version April 24, 2015. This work was supported by the Engineering and Physical Sciences Research Council under Project MIGRATION (EP/L01162X/1). The work of G. Z. Mashanovich was supported by the Royal Society through his University Research Fellowship. The work of R. Soref was supported by the Air Force Office of Scientific Research under Grant FA9550-14-1-019. Corresponding author: M. Nedeljkovic (e-mail: M.Nedeljkovic@soton.ac.uk).

**Abstract:** Germanium is becoming an important material for mid-infrared photonics, but the modulation mechanisms in Ge are not yet well understood. In this paper, we estimate the size of free-carrier electroabsorption and electrorefraction effects in germanium across the 2- to 16-$\mu$m wavelength range at 300 K. The predictions are based as much as possible upon experimental absorption data from the literature and are supported by extrapolations from experimental data using first-principle quantum theoretical modeling. We find that free-carrier absorption is substantially stronger in Ge than in Si.

**Index Terms:** Electrooptic effects, photonics.

## 1. Introduction

Germanium is becoming an increasingly more important material for photonics, especially in the mid-infrared [1], due to its transparency over a wide wavelength range (2–16.7 $\mu$m) [2]. The material also exhibits other properties that make it an attractive target for photonics, namely a high refractive index (n = 4.0–4.1 for wavelengths of 2–20 $\mu$m) [3], a large $\chi_3$ nonlinearity [4], [5], high carrier mobility [6], and it is compatible with silicon processing. The first germanium on silicon (Ge-on-Si) waveguides for the mid-infrared were demonstrated in 2012 [7], and since then Ge-on-Si waveguides with losses $<$ 1 dB/cm have been realized [8], as well as Ge-on-Si spectrometers [9] and multimode interferometers [8].

Modulation is a key function in photonic systems, which has not yet been adequately addressed in Ge. Like silicon, Ge has a centrosymmetric crystalline structure and therefore has a very weak Pockels effect and Kerr effect, while the Franz–Keldysh effect is not significant for wavelengths longer than $\sim$1.6 $\mu$m, therefore useful modulation mechanisms in Ge are likely to be the thermo-optic effect [10], [11], which is $\sim 3\times$ greater than that in silicon [12] but is relatively slow, and the free-carrier plasma effect. So far, free-carrier absorption modulation in Ge waveguides has been demonstrated experimentally only by pumping a Ge waveguide with below-bandgap light to generate free carriers [13].

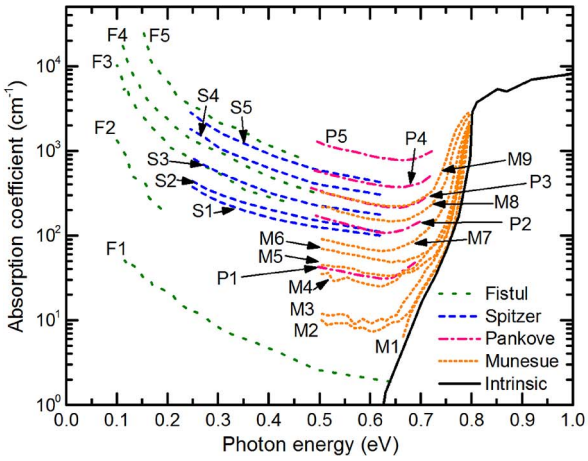


| Curve | $N_e$ ($cm^{-3}$) | Curve | $N_e$ ($cm^{-3}$) |
|---|---|---|---|
| P1 | 5.0E+18 | F3 | 1.4E+19 |
| P2 | 8.0E+18 | F4 | 1.8E+19 |
| P3 | 1.2E+19 | F5 | 3.6E+19 |
| P4 | 2.3E+19 | M1 | 3.6E+17 |
| P5 | 4.0E+19 | M2 | 2.0E+18 |
| S1 | 1.1E+19 | M3 | 4.0E+18 |
| S2 | 9.7E+18 | M4 | 1.1E+19 |
| S3 | 2.1E+19 | M5 | 1.9E+19 |
| S4 | 4.7E+19 | M6 | 3.1E+19 |
| S5 | 4.1E+19 | M7 | 1.9E+18 |
| F1 | 8.0E+17 | M8 | 5.4E+18 |
| F2 | 4.8E+18 | M9 | 6.7E+18 |

Fig. 1. N-type doped Ge absorption spectra from the literature. The references for each curve group are “Fistul” [21], “Spitzer” [19], “Pankove” [18], Munesue [20], and “Intrinsic” [25]. The table to the right shows the n-type dopant concentration of each sample.

The free-carrier plasma effect (abbreviated here as FCE for free-carrier effect) relies on altering the electron and hole concentration in crystalline germanium, which alters the absorption coefficient $(\Delta\alpha)$ and the refractive index $(\Delta n)$ of the bulk material. In silicon the electroabsorption and electrorefraction due to a change in charge carrier concentrations can be calculated from simple expressions for $\Delta\alpha$ versus $\Delta N_e$ and $\Delta N_h$, and $\Delta n$ versus $\Delta N_e$ and $\Delta N_h$ at near-infrared (NIR) [14] and mid-infrared (MIR) [15] wavelengths, which have been calculated from absorption spectra of doped silicon wafers, and from using Kramers–Kronig (KK) equations to calculate the refractive index change at different charge carrier concentrations. In this paper we adopt a similar approach for germanium, using absorption spectra of doped germanium from the literature as much as possible.

To be specific, we determine $\Delta\alpha_e$, $\Delta\alpha_h$, $\Delta n_e$ and $\Delta n_h$, where $\Delta\alpha_e = \alpha_e(\hbar\omega, N_e) - \alpha_i(\hbar\omega, N_i)$ and $\Delta\alpha_h = \alpha_h(\hbar\omega, N_h) - \alpha_i(\hbar\omega, N_i)$ where the absorption $\alpha_i$ of intrinsic Ge is taken as zero over the wavelength range of interest, and where $\alpha_e$ and $\alpha_h$ are the experimental doped-Ge values. Then we found $\Delta n_{e,h}$ using the KK integral with $\Delta\alpha_{e,h}$ in the numerator of the integrand as shown below. Because absorption spectra over the photon energy range 0 to $\infty$ are required for KK and the availability of experimental data is limited in some parts of the spectrum, we use a first-principles quantum theoretical model to extrapolate from these data over a broader wavelength range. Throughout this work, we have assumed that the temperature is 300 K and that there is no strain in the Ge. The hybrid empirical/theoretical absorption spectra are used as the inputs to Kramers–Kronig equations, in order to calculate the dependence of refractive index on charge carrier concentration. As shown here, Ge has a significant FCE advantage over Si.

## 2. Modeling Absorption in Germanium

Free-carrier absorption can most simply be modelled using the Drude theory for simple classical conductivity of charge-carriers under an applied optical electric field. However, it has been noted that the Drude model is inadequate for fully describing free carrier absorption [16], [17], and some of its shortcomings can be seen in the absorption spectra of Ge that are available in the literature.

### 2.1. Literature Review of Doped Ge Absorption Spectra

The Drude model in its simplest form predicts a $\lambda^2$ dependence of the free-carrier absorption, and although in reality the power dependence differs from this slightly, the predicted smooth increase of the absorption spectrum of n-type Ge with increasing wavelength (decreasing photon energy) can be seen in the experimental absorption spectra. Figs. 1 and 2 show a selection of

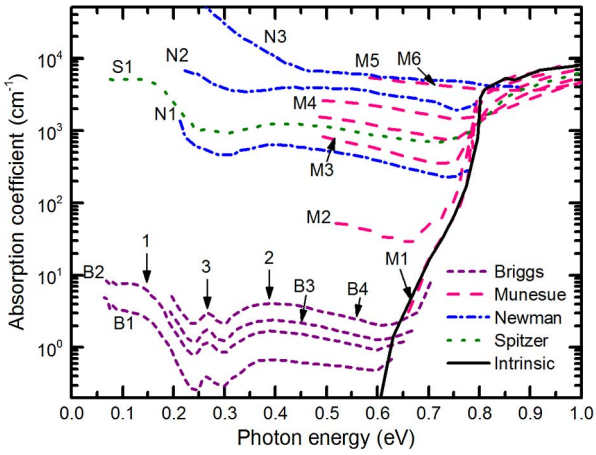


| Curve | $N_h$ (cm$^{-3}$) |
|---|---|
| B1 | 4.5E+15 |
| B2 | 1.1E+16 |
| B3 | 1.6E+16 |
| B4 | 2.2E+16 |
| N1 | 1.0E+19 |
| N2 | 6.0E+19 |
| N3 | 1.5E+20 |
| S1 | 1.1E+19 |
| M1 | 1.0E+14 |
| M2 | 4.2E+17 |
| M3 | 7.1E+18 |
| M4 | 1.4E+19 |
| M5 | 2.9E+19 |
| M6 | 8.9E+19 |

Fig. 2. P-type doped Ge absorption spectra from the literature. The references for each curve group are "Briggs" [22], "Munesue" [20], "Newman" [24], "Spitzer" [19], and "Intrinsic" [25]. The table to the right shows the p-type dopant concentration of each sample.

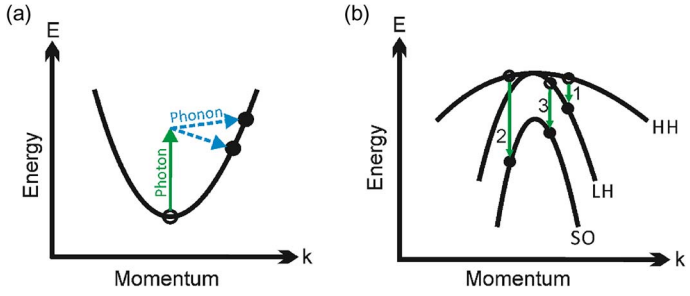


Fig. 3. (a) Intravalley free-carrier absorption process diagram. A photon is raised to a higher energy level within the same band, assisted by a phonon. (b) Intervalence band free-carrier absorption, where there is a direct hole transition between different valence bands (HH = heavy hole, LH = light hole, and SO = split-off band).

the collated absorption spectra for n- and p-type Ge, respectively, which have been digitised from [18]–[24], and where needed their scales have been transformed to be plotted in terms of photon energy (eV) on the x-axis and absorption coefficient $(\mathrm{cm}^{-1})$ on the y-axis. The absorption spectrum of intrinsic Ge from [25] is also plotted in both figures.

The absorption in Fig. 1 at photon energies smaller than the fundamental indirect absorption edge (i.e., $\hbar\omega < \sim 0.66$ eV) is due to intravalley transitions, where an absorbed photon causes a charge carrier to be raised to a higher energy level within the conduction band. It is an indirect process, which relies on scattering from the lattice or from ionized impurities for momentum conservation, as shown in Fig. 3(b).

In p-type Ge the similar process of intravalley free-carrier absorption due to intravalence band transitions is significant, but it is clear from experimental p-type spectra that absorption bands arising from other mechanisms dominate the absorption spectrum throughout the NIR and MIR, and these absorption bands are not predicted by Drude theory.

The literature data show that the absorption bands centred at 0.15 eV, 0.27 eV, and 0.4 eV are dependent on the doping concentration. Investigation of compensated material in the literature has shown that the absorption bands are the result of holes, not the dopant [22], and it is now known that these bands are due to intervalence band transitions [23], [26]. The structure of the valence bands is shown in Fig. 3(b), and the transitions between the three bands are labeled on both Figs. 2 and 3(b).

TABLE 1

Material constants of germanium from the literature, which are used in the theoretical model

| Parameter | Symbol | Value | Literature reference |
|---|---|---|---|
| Γ-valley effective mass | $m_\Gamma$ | $0.042m_0$ | [29] |
| L-valley effective mass | $m_L$ | $0.22m_0$ | [29] |
| Γ-valley edge energy | $E_\Gamma$ | 0.8 eV | [21] |
| L-valley edge energy | $E_L$ | 0.66 eV | [21] |
| Optical phonon energy | $\hbar\omega_0$ | 37 meV | [30, 31] |
| Optical phonon deformation potential constant (electrons) | $D_{0,e}$ | $5.5\times10^{10}$ eV/m | [27, 31] |
| Optical phonon deformation potential constant (holes) | $D_{0,h}$ | $8.7\times10^{10}$ eV/m | [32-34] |
| Acoustic phonon deformation potential (electrons) | $\Xi_e$ | 8.8 eV | [35] |
| Acoustic phonon deformation potential (holes) | $\Xi_h$ | 7.4 eV | [35] |
| Velocity of sound | $v_s$ | $4.18\times10^3$ m/s | [36] |
| Material density | $\rho_L$ | $5.323\times10^3$ kg/m$^3$ | [37] |
| Static dielectric constant | $K_s$ | 16 | [6] |

[1] $D_{0,h}$ was calculated using the expression $D_0 = \sqrt{\frac{3}{2}}\frac{d_0}{a_0}$, with $d_0 = 41.75$eV from [32] and $a_0 = 5.6575$Å from [34].

### 2.2. Theoretical Models

The total free-carrier absorption can be calculated by summation of all of the contributing free-carrier dependent absorption processes. For electrons in unstrained Ge, the intravalley absorption is the only significant mechanism (although we also briefly discuss indirect inter conduction band free-carrier absorption in this section), while for holes, both the intravalley and intervalley free carrier absorptions must be considered.

#### 2.2.1. Intravalley Free-Carrier Absorption

We model the intravalley component of the free-carrier absorption (FCA) using the theoretical model of Tsai *et al.* [17], which is based on the second order perturbation theory of quantum mechanics. This model has previously been applied by Wang *et al.* [27] to the case of n-type Ge. In intravalley FCA the absorption is an indirect process, where absorption of a photon raises a carrier to a higher energy level within the same band, assisted by a phonon for momentum conservation. In the Tsai theory the interactions between carriers and the different phonon types (polar optical phonon, deformation potential optical phonon, deformation potential acoustic phonon, piezoelectric acoustic phonon and charged impurity) during the intravalley transition are considered. In the case of Ge the polar optical phonon and piezoelectric phonon can be neglected due to the material's centrosymmetric crystal structure. Absorption assisted by impurities is not included in the final calculation, because for this work we are interested predominantly in cases where the charge carrier concentrations, and the associated absorption coefficient and refractive index change, are changing independently of the impurity concentration. The Tsai FCA model improves on previous theoretical models of the effect [16], [28] by accounting for the state-filling effect and degenerate carrier distribution. Table 1 shows the values of the material constants used with the model, alongside the sources of the data.

#### 2.2.2. Intervalence Band Free-Carrier Absorption

Intervalence band transitions in p-type Ge are direct transitions of carriers between the heavy hole (HH), light hole (LH), and split-off spin orbit (SO) bands. Basu [38] gives the optical

absorption due to transitions between a band $i$ to a band $j$ as

$$\propto_{ij}(\hbar\omega) = C\sum_{k_i,k_j}\left\langle|M_{ij}|^2\right\rangle\left(f_i(k)-f_j(k)\right)\delta\left(E_j(k)-E_i(k)+\hbar\omega\right)\delta_{k_i,k_j} \tag{1}$$

where $C$ is a dimensionless constant, $k$ is the momentum wavevector, $f_i$ and $f_j$ are the occupational probabilities of the two bands, and $E_i$ and $E_j$ are the energies of the two bands. The first $\delta$ is the Dirac delta function, and the $\delta_{k_i,k_j}$ is the Kronecker delta function, where $\delta_{k_i,k_j}=1$ when $k_i=k_j$, and $\delta_{k_i,k_j}=0$ when $k_i\neq k_j$. This reduces the summation over $k_i$ and $k_j$ to a single summation over $k$ [38], and effectively restricts allowed transitions to only direct transitions. $\langle|M_{ij}|^2\rangle$ is the square of the interaction matrix element between the initial and final states of carriers averaged over all directions (valid if we assume random light polarization) and is given by

$$\left\langle|M_{ij}|^2\right\rangle = \hbar^2k^2A_{ij} \tag{2}$$

where $A_{ij}$ is a dimensionless parameter that is dependent on which two bands the transition is occurring between. Following Basu, we convert the summation in (2) into an integral using the prescription

$$\sum_k \rightarrow \left(\frac{2V}{8\pi^3}\right)\int 4\pi k^2dk. \tag{3}$$

Equation (1) can then be rewritten as

$$\propto_{ij}(\hbar\omega) = C_{ij}\int k^4\left(f_i(k)-f_j(k)\right)\delta\left(E_j(k)-E_i(k)+\hbar\omega\right)dk. \tag{4}$$

We calculate the occupational probabilities $f_i$ and $f_j$ using the Fermi–Dirac distribution function of carriers, for consistency with the Tsai theory, and to account for the degenerate carrier case. In his consideration Basu uses the parabolic band approximation for calculation of the energy bands, but we find in practice that when a non-parabolic band structure is used the shape of the theoretically calculated bands much more closely matches the shape of experimentally measured absorption bands. The non-parabolic band structure is calculated with the analytical expressions for the valence bands of Ge produced by Rodriguez-Bolivar *et al.* [39], which are fits to the results of rigorous theoretical band structure calculations based on the pseudopotential method. The carrier distribution function is also modified to reflect the non-parabolicity following the method of Rodriguez-Bolivar *et al.* [39].

We also found that incorporating the effect of temperature dependent lifetime broadening into the model substantially improved the agreement with literature data, which has previously been noted for the case of p-type absorption in Ge at low temperatures in [40]. We do this by replacing the Dirac delta function in (4) with a Lorentzian probability density function so that

$$\propto_{ij}(\hbar\omega) = C_{ij}\int k^4\left(f_i(k)-f_j(k)\right)L\left(E_j(k)-E_i(k)+\hbar\omega\right)dk \tag{5}$$

$$L\left(E_j(k)-E_i(k)+\hbar\omega\right) = \frac{\gamma}{\pi\left[\left(E_j(k)-E_i(k)+\hbar\omega\right)^2+\gamma^2\right]} \tag{6}$$

where $\gamma$ is the parameter that determines the width of the broadening.

### 2.2.3. Far-Infrared Free-Carrier Absorption

In the far-infrared wavelength region the absorption spectrum of doped silicon is known from experimental data to saturate [41], [42], and the same process can be expected to occur in Ge both from classical theory [42] and in the quantum mechanical description [16]. According to the explanation of [16], in the far-infrared the energy of optical photons becomes comparable to,

and eventually smaller than, the energy of phonons; therefore, absorption assisted by phonon absorption is no longer possible, but absorption assisted by phonon emission is possible. The phonon emission assisted optical absorption is approximately inversely proportional to the square of the phonon frequency, which is finite and constant. There is therefore a far-IR saturation of the free-carrier absorption spectrum. However, the theory applied in the Tsai *et al.* model does not incorporate this effect, therefore in this work a saturation is implemented by artificially applying a levelling off of the absorption spectra for wavelengths smaller than the optical phonon energy, $\hbar\omega_0$, and using a moving average window filter to smooth the curve near the discontinuity.

#### 2.2.4. Indirect Interband Free-Carrier Absorption

In some materials, e.g., Si and GaAs, there are significant absorption bands in the n-type absorption spectra that are the result of indirect intervalley FCA, resulting when an electron is raised to a higher energy level in a different valley of the conduction band, assisted by a phonon. We estimated the size of this effect using the Tsai *et al.* theoretical model [17] and found that absorption arising from this effect was negligible compared to intravalley FCA. The material constants in Table 1 were used in this calculation. This conclusion is supported by the shape of the n-type Ge absorption spectra, which corresponds well to that expected from intravalley FCA. It is worth noting that this may only be true for unstrained Ge; in [27], the absorption spectrum of n-type tensile strained Ge was measured, and displayed a response in one part of the spectrum that was ascribed to intervalley absorption.

### 2.3. Merging Experimental and Theoretical Absorption Spectra

#### 2.3.1. N-Type Ge Absorption Spectra

For n-type Ge the shape of the theoretically calculated absorption spectra agreed well with the literature spectra. However, there were slight discrepancies between the magnitudes of theoretical absorption curves and experimental absorption curves with the same charge-carrier concentrations. Additionally, there were discrepancies between curves of similar charge carrier concentrations from both the same data sets and from different literature sources. Therefore, a multiplication factor was introduced as a fitting parameter into the theoretical absorption model. The theoretical model was fitted to each experimental curve using a numerical nonlinear curve fitting method [43], and the fitted multiplication factor was recorded for each curve. For this fitting the absorption due to charged impurities was included in the total absorption, to reflect the case of doped germanium, where the impurity concentration can be assumed to be equal to the free-carrier concentration. Note that which element is used as the N-type dopant does not affect this calculation. The value of the multiplication factor used for final calculations was 2.08, which was the median of all of the fitting parameters. There was no clear correlation between the fitted multiplication factor and charge-carrier concentration. When calculating the final free-carrier absorption the absorption resulting from charged impurities was neglected. Finally, the far-infrared saturation was applied as described previously. The adjusted theoretical free-carrier absorption spectra for different electron concentrations are shown in Fig. 4.

#### 2.3.2. P-Type Ge Absorption Spectra

The shapes of the heavy hole to light hole and heavy hole to split-off band absorptions could be satisfactorily reproduced only when fitting parameters were introduced. The fitting parameters that were used were the multiplying factors $C_{HL}$ and $C_{LS}$ from (3), the spherical coordinate angles in K space $\theta$ and $\phi$, which appear in the Rodriguez-Bolivar *et al.* [39] models for the nonparabolic valence band structures, and the $\gamma$ factor in the Lorentzian broadening. Additionally, a multiplying factor A was introduced to the intravalley FCA, as in the calculation of n-type absorption.

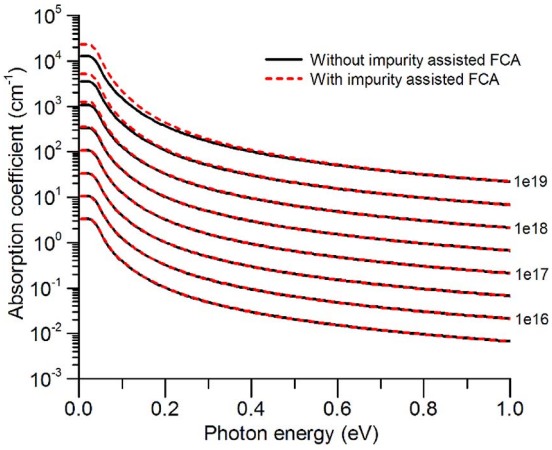


Fig. 4. N-type adjusted theoretical absorption spectra.

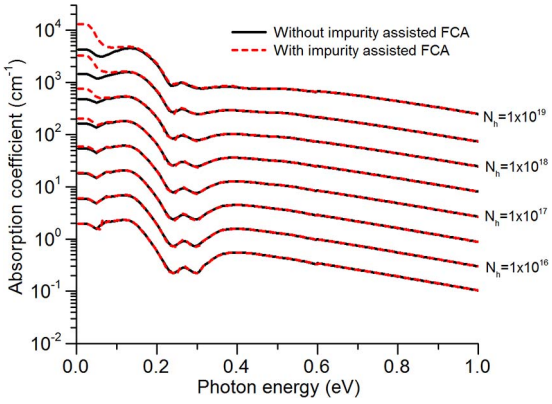


Fig. 5. P-type hybrid literature and theoretical absorption spectra.

In this work, the absorption at photon energies in the range 0.1 eV–0.6 eV was found by interpolation of the literature absorption spectra in Fig. 2. For extrapolation to higher photon energies the theoretical spectrum is fitted to the interpolated spectrum over the range 0.4–0.6 eV, using the parameters $C_{HS}$, $\gamma$, $\theta$ and $\phi$. Using the fitted parameters the theoretical spectrum is calculated from 0.6 eV to 3.0 eV, and the join between the two curves is smoothed using a simple moving average window filter. For low photon energies the same process is used, but in this case the parameters $C_{HL}$, $\gamma$, $\theta$, $\phi$ and A are fitted over the range 0.1 eV to 0.2 eV. Again the calculated absorption is used to extrapolate to lower photon energies, and the joins between the curves are smoothed. In the far-IR a saturation is implemented in the same way as for n-type Ge.

In Fig. 5 the resulting change in absorption coefficient spectra are plotted for several charge carrier concentrations in the range $3.2 \times 10^{15} - 1 \times 10^{19}$ cm$^{-3}$. The absorption has been plotted both for the case where impurity assisted absorption is included, which is the case for doped Ge, and without this absorption, which corresponds to the case of charge-carrier injection or depletion.

The significant sources of possible error in the calculation of these absorption spectra arise predominantly from the scarcity of available data in the literature, particularly in the far-infrared region of the spectrum, below 0.1 eV. Therefore the fitting relies on only a few data points, and we are unable to verify the level and wavelength of the far-IR saturation. Additionally, for both n-type and p-type Ge the theory appears to underestimate the intravalley FCA absorption. This

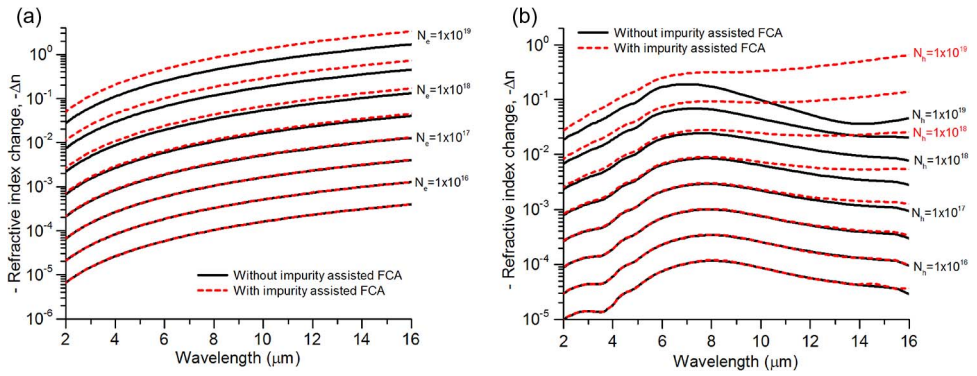


Fig. 6. Calculated refractive index spectra at 300° K for (a) N-type Ge and (b) P-type Ge.

may be because the Tsai *et al.* theoretical model does not account for the nonparabolicity of the Ge band structure. However, further experimental or theoretical work is required to determine whether the discrepancy is the result of errors in the calculation of the absorption due to optical phonons, acoustic phonons, or charged impurities, or whether there are any experimental measurement errors. A complicating factor might be that in some heavily doped samples the impurity concentration and charge-carrier concentration are not equal due to incomplete ionization of impurity atoms [21], which can depend on the dopant used.

However, the spectra in Figs. 4 and 5 represent the most complete data currently available for the change in absorption coefficient due to charge carriers, and following the hybrid experimental/theoretical approach allows for the influence of ionized impurities on free-carrier absorption to be removed.

## 3. Refractive Index Change Calculation

The change in refractive index was calculated from the hybrid absorption coefficient spectra at discrete electron and hole concentrations in the range $1.8 \times 10^{15}$ cm$^{-3}$ to $1.0 \times 10^{19}$ cm$^{-3}$ using Kramers–Kronig equations. The change in refractive index and change in absorption coefficient are related by

$$\Delta n(v) = 6.3 \times 10^{-6}(\text{cm.V})P \int_0^{\infty} \frac{\Delta \propto (V')dV'}{V'^2 - V^2} \tag{7}$$

where $V$ is the normalized photon energy, defined as $V = \hbar\omega/e$, (cm.V) is the unit for the factor outside the integral, and $P$ indicates that the principal part of the integral must be taken, as there is a singularity at $V' = V$. The Kramers–Kronig integration was carried out by a trapezoidal rule integration method, as previously described in [15], over the photon energy range 0–3 eV, with increments of 0.005 eV. The resulting spectra are shown in Fig. 6(a) for electrons and in Fig. 6(b) for holes. In both figures spectra have been plotted with and without the effect of charged impurities on absorption.

Charged impurities can be seen to have a significant effect on $\Delta n$ for electrons for concentrations greater than approximately $N_e = 1 \times 10^{18}$ cm$^{-3}$, and for holes above $N_h = 1 \times 10^{17}$ cm$^{-3}$. For holes, when charged impurities are not included $\Delta n$ becomes positive at high carrier concentrations and long wavelengths (i.e., for $N_h = 1 \times 10^{17}$ cm$^{-3}$, $\Delta n$ is positive for 13 $\mu$m $< \lambda <$ 18 $\mu$m).

In Fig. 7, predictions of the refractive index change calculated using this method are compared to experimentally measured values of the refractive index from literature [23] of a heavily doped p-type Ge wafer with $N_h = 1.1 \times 10^{19}$ cm$^{-3}$ over the range 7.8 $\mu$m $> \lambda >$ 19 $\mu$m and of a heavily doped n-type Ge wafer with $N_e = 3.9 \times 10^{18}$ cm$^{-3}$ over the range 2.7 $\mu$m $> \lambda >$ 23 $\mu$m.

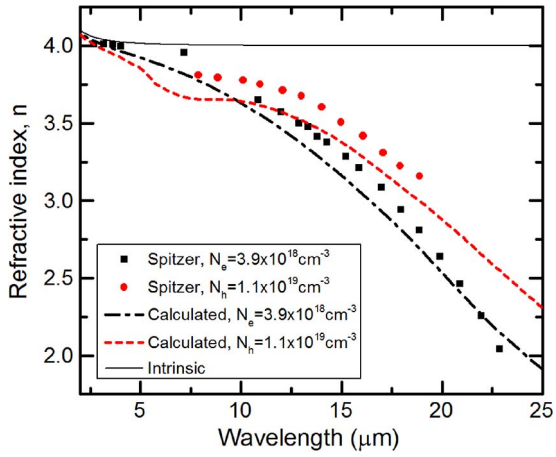


Fig. 7. Comparison of calculated refractive index for doped Ge and experimental measurements of refractive index from [23], for p-type Ge with $\Delta N_h = 1.1 \times 10^{19}$ cm$^{-3}$ and n-type Ge with $N_e = 3.9 \times 10^{18}$ cm$^{-3}$. Calculated values for $\Delta n$ due to doping are subtracted from refractive index data of intrinsic Ge from [3]. Calculated curves include absorption resulting from charged impurity scattering.

The calculated change in refractive index values for those same carrier concentrations, which include the charged impurity contribution to free-carrier absorption, have been added to the refractive index spectrum of intrinsic Ge from [3], and are plotted on the same graph.

The comparison of the predicted data and literature data shows an agreement of the order of magnitude of $-\Delta n$ for both electrons and holes. However, the p-type Ge model overestimates $-\Delta n$ compared to the literature spectrum, particularly at the lower end of the wavelength range, and there is no p-type data for $\lambda < 7.8$ $\mu$m, so it is impossible to compare the agreement in this range. For n-type Ge the discrepancy between experimental and calculated $-\Delta n$ is smaller, but the lone data point at 7.2 $\mu$m is offset from the calculated line. As with the absorption spectra, the scarcity of experimental data is a hindrance in understanding how accurate the calculated model is.

## 4. Results and Discussion

The red curves in Figs. 4–6 represent the case in which there is "background doping" that assists (adds to) the change in FCA. This corresponds to absorption spectra of doped wafers, where each absorption curve has different impurity concentrations as well as different charge carrier concentrations. Therefore the red curves for EA are effectively an extrapolation/fitting of the literature absorption spectra. Fig. 7 shows a comparison between the refractive index spectra of doped wafers from the literature and the calculated refractive index change, when changing impurity/doping concentration is included in the calculation. The black curves in Figs. 4–6 correspond to the situation in group IV EO modulators, where the impurity concentration is constant, but the charge carrier concentration is changing. The black lines are therefore preferred for device predictions, and the "device coefficients" given below have been fitted to this data. The black lines have been calculated by first fitting/extrapolating the red lines to the experimental spectra, and then subtracting the contribution of changing impurity concentration to FCA.

In order to produce a convenient design tool for modeling devices based on free-carrier absorption in Ge, equations of the simple form shown in (8) and (9), shown below, have been fitted to plots of $\Delta\alpha$ versus $\Delta N_e$, $\Delta\alpha$ versus $\Delta N_h$, $-\Delta n$ versus $\Delta N_e$ and $-\Delta n$ versus $\Delta N_h$. The fitted coefficients are shown in Table 2 for wavelengths between 2 $\mu$m and 16 $\mu$m at intervals of 0.5 $\mu$m. For $\Delta\alpha$ versus $\Delta N_e$, $\Delta\alpha$ versus $\Delta N_h$ and $-\Delta n$ versus $\Delta N_e$, the fitting has been carried out over the carrier concentration range $2 \times 10^{15}$ cm$^{-3} < \Delta N < 1 \times 10^{19}$ cm$^{-3}$. For $-\Delta n$ versus $\Delta N_h$, the upper

TABLE 2

Fitting parameters to (8) and (9), for $\Delta\alpha$ versus $\Delta N_e$, $\Delta\alpha$ versus $\Delta N_h$, $-\Delta n$ versus $\Delta N_e$ and $-\Delta n$ versus $\Delta N_h$ values from data calculated in this work, at wavelengths between 2 $\mu$m and 16 $\mu$m

| Wavelength, $\lambda$ (μm) | -Δn | | | | Δα | | | | |
|---|---|---|---|---|---|---|---|---|---|
| | *a* ($cm^2$) | *b* | *c* ($cm^2$) | *d* | *p* ($cm^3$) | *q* | *r* ($cm^3$) | *s* | *Upper $\Delta N_h$ limit for -Δn fitting equations* |
| 2 | 6.30E-18 | 1.007 | 1.03E-15 | 0.935 | 8.91E-22 | 1.023 | 2.04E-20 | 0.948 | 1E+19 |
| 2.5 | 8.63E-18 | 1.008 | 2.34E-15 | 0.922 | 1.38E-21 | 1.023 | 2.61E-20 | 0.948 | 1E+19 |
| 3 | 1.11E-17 | 1.009 | 4.99E-15 | 0.906 | 1.96E-21 | 1.023 | 1.19E-20 | 0.973 | 1E+19 |
| 3.5 | 1.38E-17 | 1.011 | 2.35E-15 | 0.924 | 2.65E-21 | 1.023 | 2.98E-21 | 1.010 | 1E+19 |
| 4 | 1.66E-17 | 1.012 | 1.25E-16 | 0.989 | 3.43E-21 | 1.024 | 4.64E-21 | 1.007 | 1E+19 |
| 4.5 | 1.96E-17 | 1.013 | 6.60E-17 | 1.008 | 4.30E-21 | 1.024 | 1.98E-20 | 0.980 | 1E+19 |
| 5 | 2.25E-17 | 1.014 | 2.63E-17 | 1.029 | 5.27E-21 | 1.024 | 3.42E-20 | 0.972 | 1E+19 |
| 5.5 | 2.57E-17 | 1.016 | 3.51E-17 | 1.026 | 6.34E-21 | 1.024 | 5.06E-20 | 0.971 | 1E+19 |
| 6 | 2.89E-17 | 1.017 | 5.94E-17 | 1.027 | 7.49E-21 | 1.024 | 8.32E-20 | 0.965 | 1E+19 |
| 6.5 | 3.22E-17 | 1.018 | 1.50E-16 | 1.013 | 8.75E-21 | 1.024 | 1.54E-19 | 0.953 | 1E+19 |
| 7 | 3.57E-17 | 1.019 | 3.53E-16 | 0.998 | 1.01E-20 | 1.024 | 2.58E-19 | 0.942 | 1E+19 |
| 7.5 | 3.94E-17 | 1.020 | 7.57E-16 | 0.984 | 1.15E-20 | 1.024 | 4.06E-19 | 0.932 | 6E+18 |
| 8 | 4.33E-17 | 1.020 | 1.50E-15 | 0.971 | 1.31E-20 | 1.025 | 5.89E-19 | 0.923 | 6E+18 |
| 8.5 | 4.73E-17 | 1.021 | 2.60E-15 | 0.960 | 1.47E-20 | 1.025 | 7.16E-19 | 0.917 | 3E+18 |
| 9 | 5.15E-17 | 1.022 | 3.81E-15 | 0.952 | 1.64E-20 | 1.025 | 7.35E-19 | 0.914 | 3E+18 |
| 9.5 | 5.62E-17 | 1.022 | 4.77E-15 | 0.947 | 1.83E-20 | 1.025 | 6.55E-19 | 0.915 | 2E+18 |
| 10 | 6.08E-17 | 1.023 | 5.33E-15 | 0.945 | 2.02E-20 | 1.025 | 5.44E-19 | 0.917 | 2E+18 |
| 10.5 | 6.58E-17 | 1.023 | 5.58E-15 | 0.943 | 2.22E-20 | 1.025 | 4.44E-19 | 0.920 | 2E+18 |
| 11 | 7.14E-17 | 1.024 | 5.61E-15 | 0.943 | 2.43E-20 | 1.025 | 3.64E-19 | 0.922 | 2E+18 |
| 11.5 | 7.65E-17 | 1.024 | 5.55E-15 | 0.943 | 2.65E-20 | 1.025 | 3.09E-19 | 0.924 | 2E+18 |
| 12 | 8.26E-17 | 1.025 | 5.49E-15 | 0.943 | 2.89E-20 | 1.025 | 2.68E-19 | 0.925 | 2E+18 |
| 12.5 | 8.95E-17 | 1.025 | 5.34E-15 | 0.944 | 3.13E-20 | 1.025 | 2.47E-19 | 0.925 | 2E+18 |
| 13 | 9.56E-17 | 1.025 | 5.29E-15 | 0.944 | 3.38E-20 | 1.025 | 2.46E-19 | 0.924 | 2E+18 |
| 13.5 | 1.02E-16 | 1.025 | 5.49E-15 | 0.942 | 3.64E-20 | 1.025 | 2.29E-19 | 0.924 | 2E+18 |
| 14 | 1.09E-16 | 1.026 | 5.59E-15 | 0.942 | 3.92E-20 | 1.024 | 2.01E-19 | 0.926 | 2E+18 |
| 14.5 | 1.18E-16 | 1.025 | 5.52E-15 | 0.942 | 4.19E-20 | 1.024 | 1.80E-19 | 0.928 | 2E+18 |
| 15 | 1.27E-16 | 1.025 | 5.71E-15 | 0.941 | 4.48E-20 | 1.024 | 1.66E-19 | 0.929 | 2E+18 |
| 15.5 | 1.34E-16 | 1.026 | 6.21E-15 | 0.938 | 4.77E-20 | 1.024 | 1.26E-19 | 0.935 | 2E+18 |
| 16 | 1.42E-16 | 1.026 | 6.85E-15 | 0.936 | 5.08E-20 | 1.024 | 5.68E-20 | 0.953 | 2E+18 |

limit of the fitting range for each wavelength is shown in the final column of the table, while the lower limit is $2 \times 10^{15}$ $cm^{-3}$.

$$\Delta \propto (\lambda) = \Delta \propto_e (\lambda) + \Delta \propto_h (\lambda) = a(\lambda)\Delta N_e^{b(\lambda)} + c(\lambda)\Delta N_h^{d(\lambda)} \tag{8}$$

$$-\Delta n(\lambda) = \Delta n_e(\lambda) + \Delta n_h(\lambda) = p(\lambda)\Delta N_e^{q(\lambda)} + r(\lambda)\Delta N_h^{s(\lambda)}. \tag{9}$$

The shape of the $-\Delta n$ versus $\Delta N_h$ trend changes at very high carrier concentrations (particularly at longer wavelengths) due to the material becoming degenerate, therefore in order to maintain simple fitting equations we simply reduce the $\Delta N_h$ range of fitting where necessary. As an example the calculated $-\Delta n$ versus $\Delta N_h$ data is shown alongside the fitted lines for different wavelengths in Fig. 8.

## 5. Comparison of FCE in Ge With FCE in Si

Looking at the absorption spectra for both p-doped Ge and p-doped Si, we see that FCA in p-Ge is fundamentally different from that in p-Si because of the intervalence-band local absorption maxima that are present only in Ge. These Ge absorption peaks or "humps" affect both ER and EA in p-Ge. There are two consequences: 1) The EA is larger in p-Ge than in p-Si, and 2) the ER in p-Ge is actually slightly weaker than that in p-Si. This occurs for reasons related

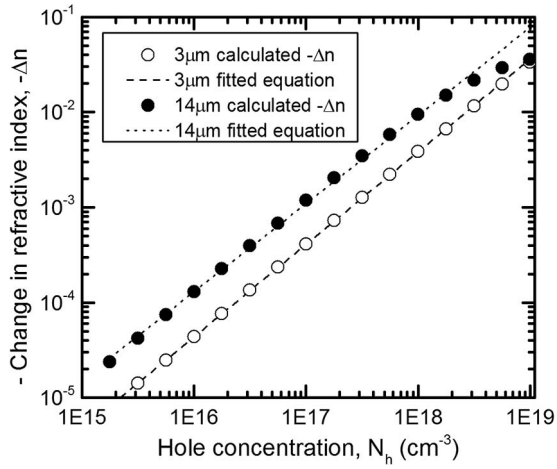


Fig. 8. Comparison of calculated data for $-\Delta n$ versus $\Delta N_h$ plotted alongside the lines drawn using the fitting parameters at $\lambda = 3$ $\mu$m and $\lambda = 14$ $\mu$m.

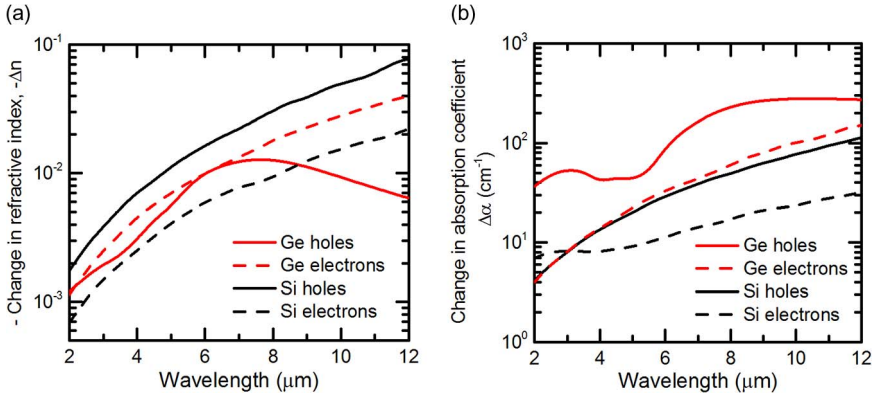


Fig. 9. Comparisons of (a) change in refractive index and (b) change in absorption coefficient at $\Delta N_e = \Delta N_h = 5 \times 10^{17}$ cm$^{-3}$ in Si and Ge.

to the KK relations. At a localized absorption peak at photon energy $\hbar\omega_p$, the induced index change $\Delta n$ has a derivative shape as a function of $\hbar\omega$ (derivative with respect to the $\alpha$-versus-$\hbar\omega$ shape). KK then dictates that the $\Delta n$ is somewhat depressed at photon energies slightly larger than $\hbar\omega_p$. Specifically, for p-Ge, there are local absorption peaks at $\hbar\omega = 0.15$, 0.27, and 0.40 eV—which in turn reduces $\Delta n$ above 0.4 eV below the $\Delta n$ that would have been present in the absence of peaks.

The wavelength range from 2 to 12 $\mu$m is a convenient one for making a quantitative comparison of FCE in Ge and Si. To give a concrete comparison, we shall assume the same level of carrier injection in both Ge and Si, namely $\Delta N_e = 5 \times 10^{17}$ cm$^{-3}$ and $\Delta N_h = 5 \times 10^{17}$ cm$^{-3}$ which is midway between the low and high injection values presented in Fig. 6(a) and (b). Now we shall examine $(n + i\Delta k/\Delta N)$ for both semiconductors. The Silicon FCE is presented in detail over the 1.3 to 14 $\mu$m range by Nedeljkovic *et al.* [15]. Table 1 in that paper is used to determine the 2–12 $\mu$m responses of Si. Table 2 of this paper predicts the Ge response.

First we plot in Fig. 9(a) the ER in these two materials ($\Delta n_e$(Ge), $\Delta n_e$(Si), $\Delta n_h$(Ge) and $\Delta n_h$(Si)) as a function of wavelength, on the same graph. It is seen that $\Delta n_h$(Ge) is smaller than$\Delta n_h$(Si), particularly for $\lambda > 7$ $\mu$m, while $\Delta n_e$(Ge) is greater than $\Delta n_e$(Si) throughout the range. Next the induced absorption is plotted versus $\lambda$ in Fig. 9(b), where $\Delta\alpha_e$ and $\Delta\alpha_h$ of Ge are both significantly stronger than the corresponding $\Delta\alpha$ in silicon.

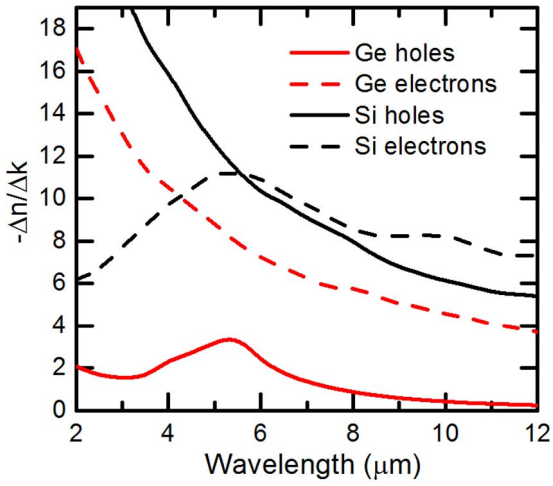


Fig. 10. Comparison of $-\Delta n/\Delta k$ at $\Delta N_e = \Delta N_h = 5 \times 10^{17}$ cm$^{-3}$ in Si and Ge.

In designing the new group IV EO modulators, it is often valuable to know the size of the induced phase shift with respect to the size of the induced amplitude shift. For that reason, we examined the ratio $-\Delta n/\Delta k$ (where $k = \alpha\lambda/4\pi$), in Ge and Si for both the electron and hole cases, with the result given in Fig. 10 where it is found that the ratio is generally smaller in Ge than in Si, particularly in p-type Ge. Additionally, $-\Delta n/\Delta$k generally decreases with wavelength. This indicates that in Ge FCE modulators exploiting electroabsorption will be more effective than those exploiting electrorefraction.

We shall close this section with a comment on the Drude model that has elsewhere been employed to catalog the relative Ge and Si behavior. Firstly, it is an implicit assumption of the model that all bands of the semiconductor are parabolic, which is an over simplification. More significantly, it ignores some free-carrier related absorption mechanisms, namely any interband absorption processes, which we have seen are significant in p-type Ge, as well as in n-type Si. This explains the discrepancies between the Soref-Friedman model [44] and the present work.

## 6. Prospects for FCE in SiGeSn

The FCE is expected to be "generally strong" in the group IV ternary alloy SiGeSn, although it is difficult to quantify this strength without going into a detailed KK analysis—a calculation requiring spectra not yet measured. The energy $E_g$ of the fundamental bandgap—whether the gap is indirect or direct—is tunable by the choice of composition $xy$ in $Si_{1-x-y}Ge_xSn_y$ (that is, $E_g$ is tunable "by design") and the cubic lattice parameter can be varied independently [45]. The attainment of a direct bandgap is governed mainly by the tin content of the ternary. Typically, directness is found for a tin fraction above 9%. This materials system is the foundation of a silicon-based SiGeSn heterostructure technology in which a complete suite of integrated optical components, both active and passive, can in principle be built on silicon using these group IV alloys [46]. Single mode SiGeSn channel waveguide designs are now available for the midwave/longwave infrared [47], and the range of transparency (high transmission) can be 2 to 20 $\mu$m, for example, with the starting wavelength dependent upon bandgap ($\hbar\omega > E_g$). Therefore, in association with such waveguides, we anticipate that SiGeSn waveguide core material is a prime candidate for a new type of free-carrier electrooptical modulator situated in the monolithic CMOS-compatible group IV chip. Taking the example of a GeSn FCE modulator possessing about 10% Sn content, we expect that the GeSn FCE core-response will be *slightly stronger than that of Ge* and will have electrooptical application at wavelengths beyond 2.8 $\mu$m.

We shall close this section with a comment on the carrier-related plasmonic properties of Ge and SiGeSn. It is shown above for Ge (and by extension SiGeSn) that heavily "injected" Ge

experiences a strong modification of its $n + i\Delta k$ index, $n'' + i\Delta k'' = n - \Delta n + i(k + \Delta k)$ being the perturbed index. Because the $\Delta n$ and $\Delta k$ perturbation is large and increases with increasing wavelength, it is clear that the real permittivity $\varepsilon_r$ of the SiGeSn will become negative above a threshold wavelength and threshold injection since $\varepsilon_r = n'^2 - k'^2$. This negative-$\varepsilon$ "crossover" occurs at the plasmonic resonance wavelength $(\lambda_p)$. Then, at $\lambda > \lambda_p$, the SiGeSn becomes a practical "plasmonic conductor", taking the place of a metal in a composite metal/dielectric structure that could be deployed in plasmonic waveguides devices [48]. Therefore, our free carrier analysis also highlights some plasmonic-photonic possibilities.

## 7. Conclusion

We have produced predictions of the free carrier effect in germanium, in order to facilitate the design of electrically controlled structures exploiting FCE in Ge throughout the 2–16 $\mu$m wavelength range. The predictions lead to the conclusion that Ge modulators exploiting free-carrier electroabsorption are likely to be more effective than those using electrorefraction.

The predictions are based partly on experimental data for N- and P-doped Ge absorption from various literature sources, and partly on first principles theoretical calculations. We see relatively good agreement between experiment and theory, but ultimately more experimental data is needed to test the validity of these predictions and to improve their accuracy. The predictions in this paper represent the most complete prediction of the free-carrier effect in Ge in the mid-infrared so far.

In further work, it would be very useful to investigate the effect of introducing strain in Ge upon the free-carrier effect.

## References


[1] R. Soref, "Mid-infrared photonics in silicon and germanium," *Nature Photon.*, vol. 4, pp. 495–497, 2010.

[2] R. A. Soref, S. J. Emelett, and W. R. Buchwald, "Silicon waveguided components for the long-wave infrared region," *J. Opt. A, Pure Appl. Opt.*, vol. 8, no. 10, pp. 840–848, Oct. 2006.

[3] H. H. Li, "Refractive index of silicon and germanium and its wavelength and temperature derivatives," *J. Phys. Chem. Ref. Data*, vol. 9, no. 3, pp. 561–658, Jul. 1980.

[4] N. K. Hon, R. Soref, and B. Jalali, "The third-order nonlinear optical coefficients of Si, Ge, and $Si_{1-x}Ge_x$ in the mid-wave and longwave infrared," *J. Appl. Phys.*, vol. 110, no. 1, Jul. 2011, Art. ID. 011301.

[5] C. Wolff, R. Soref, C. G. Poulton, and B. J. Eggleton, "Germanium as a material for stimulated Brillouin scattering in the mid-infrared," *Opt. Exp.*, vol. 22, no. 25, pp. 30735–30747, Dec. 2014.

[6] S. M. Sze and J. C. Irvin, "Resistivity, mobility and impurity levels in GaAs, Ge, and Si at 300° K," *Solid-State Electron.*, vol. 11, no. 6, pp. 599–602, 1968.

[7] Y.-C. Chang, V. Paeder, L. Hvozdara, J.-M. Hartmann, and H. P. Herzig, "Low-loss germanium strip waveguides on silicon for the mid-infrared," *Opt. Lett.*, vol. 37, no. 14, pp. 2883–2885, Jul. 2012.

[8] M. Nedeljkovic *et al.,* "Surface grating coupled low loss Ge-on-Si rib waveguides and multimode interferometers," *IEEE Photon. Technol. Lett.*, to be published, [Online]. Available: http://ieeexplore.ieee.org/xpl/articleDetails.jsp?arnumber=7045441

[9] G. Roelkens *et al.,* "Silicon-based photonic integration beyond the telecommunication wavelength range," *IEEE J. Sel. Topics Quantum Electron.*, vol. 20, no. 4, pp. 394–404, Jul./Aug. 2014.

[10] A. Malik *et al.,* "Ge-on-Si and Ge-on-SOI thermo-optic phase shifters for the mid-infrared," *Opt. Exp.*, vol. 22, no. 23, pp. 28479–28488, Nov. 2014.

[11] M. Nedeljkovic *et al.,* "Mid-infrared thermo-optic modulators in SoI," *IEEE Photon. Technol. Lett.*, vol. 26, no. 13, pp. 1352–1355, Jul. 2014.

[12] B. J. L. Frey, B. Douglas, and T. J. Madison, "Temperature-dependent refractive index of silicon and germanium," in *Proc. SPIE*, Greenbelt, MD, USA, 2004, pp. 1–10.

[13] L. Shen *et al.,* "Mid-infrared all-optical modulation in low-loss germanium-on-silicon waveguides," *Opt. Lett.*, vol. 40, no. 2, pp. 268–271, Jan. 2015.

[14] R. A. Soref and B. R. Bennett, "Electrooptical effects in silicon," *IEEE J. Quantum Electron.*, vol. QE-23, no. 1, pp. 123–129, Jan. 1987.

[15] M. Nedeljkovic, R. Soref, and G. Z. Mashanovich, "Free-carrier electrorefraction and electroabsorption modulation predictions for silicon over the 1.3–14 um infrared wavelength range," *IEEE Photon. J.*, vol. 3, no. 6, pp. 1171–1180, Dec. 2011.

[16] H. C. Huang, S. Yee, and M. Soma, "Quantum calculations of the change of refractive index due to free carriers in silicon with nonparabolic band structure," *J. Appl. Phys.*, vol. 67, no. 4, pp. 2033–2039, Feb. 1990.

[17] C.-Y. Tsai *et al.,* "Theoretical model for intravalley and intervalley free-carrier absorption in semiconductor lasers: Beyond the classical Drude model," *IEEE J. Quantum Electron.*, vol. 34, no. 3, pp. 552–559, May 1998.

[18] J. I. Pankove and P. Aigrain, "Optical absorption of arsenic-doped degenerate germanium," *Phys. Rev.*, vol. 126, no. 3, pp. 956–962, May 1962.
[19] W. G. Spitzer, F. A. Trumbore, and R. A. Logan, "Properties of heavily doped n-type germanium," *J. Appl. Phys.*, vol. 32, no. 10, pp. 1822–1830, Oct. 1961.
[20] M. Seiji and A. Toshihiro, "The intrinsic absorption edge of heavily doped N- and P-type germanium," *Jpn. J. Appl. Phys.*, vol. 3, no. 5, p. 269, 1964.
[21] V. I. Fistul', "Optical properties of heavily doped semiconductors," in *Heavily Doped Semiconductors*, vol. 1. New York, NY, USA: Springer-Verlag, 1969, pp. 207–244.
[22] H. B. Briggs and R. C. Fletcher, "New infrared absorption bands in p-type germanium," *Phys. Rev.*, vol. 87, no. 2, pp. 1130–1131, Sep. 1952.
[23] W. G. Spitzer and H. Y. Fan, "Determination of optical constants and carrier effective mass of semiconductors," *Phys. Rev.*, vol. 106, no. 5, pp. 882–890, Jun. 1957.
[24] R. Newman and W. W. Tyler, "Effect of impurities on free-hole infrared absorption in p-type germanium," *Phys. Rev.*, vol. 105, no. 3, pp. 885–886, Feb. 1957.
[25] W. C. Dash and R. Newman, "Intrinsic optical absorption in single-crystal germanium and silicon at 77° K and 300° K," *Phys. Rev.*, vol. 99, no. 4, pp. 1151–1155, Aug. 1955.
[26] H. B. Briggs and R. C. Fletcher, "Absorption of infrared light by free carriers in germanium," *Phys. Rev.*, vol. 91, no. 6, pp. 1342–1346, Sep. 1953.
[27] X. Wang *et al.,* "Infrared absorption of n-type tensile-strained Ge-on-Si," *Opt. Lett.*, vol. 38, no. 5, pp. 652–654, Mar. 2013.
[28] B. K. Ridley, Quantum Processes in Semiconductors, 5th ed. Oxford, U.K.: Oxford Univ. Press, 2013.
[29] V. Palankovski, "*Simulation of heterojunction bipolar transistors*," Ph.D. dissertation, Fakultät Elektrotechnik Informationstechnik, Techn. Univ. Wien, Wien, Germany, 2000.
[30] J. Singh, *Physics of Semiconductors and Their Heterostructures*. New York, NY, USA: McGraw-Hill, 1993.
[31] S. Smirnov, "Physical modeling of electron transport in strained silicon and silicon-germanium," Ph.D. dissertation, Fakultät Elektrotechnik Informationstechnik, Techn. Univ. Wien, Wien, Germany, 2003.
[32] M. V. Fischetti and S. E. Laux, "Band structure, deformation potentials, and carrier mobility in strained Si, Ge, and SiGe alloys," *J. Appl. Phys.*, vol. 80, no. 4, pp. 2234–2252, Aug. 1996.
[33] S. K. Chun, "Optical deformation potential constant for non-polar optical phonon scattering in the valence band of alloy semiconductors," *J. Korean Phys. Soc.*, vol. 39, no. 2, pp. 340–343, Aug. 2001.
[34] J. P. Dismukes, L. Ekstrom, and R. J. Paff, "Lattice parameter and density in germanium–silicon alloys," *J. Phys. Chem.*, vol. 68, no. 10, pp. 3021–3027, Oct. 1964.
[35] G. Karlowatz, "Advanced Monte Carlo simulation for semiconductor devices," Ph.D. dissertation, Fakultät Elektrotechnik Informationstechnik, Techn. Univ. Wien, Wien, Germany, 2009.
[36] G. V. Samsonov, *Handbook of the Physicochemical Properties of the Elements*. New York, NY, USA: Springer-Verlag, 1968.
[37] E. M. Conwell, "Properties of silicon and germanium," *Proc. IRE*, vol. 40, no. 11, pp. 1327–1337, Nov. 1952.
[38] P. K. Basu, *Theory of Optical Processes in Semiconductors: Bulk and Microstructures*. Oxford, U.K.: Oxford Univ. Press, 1997.
[39] S. Rodríguez-Bolívar, F. M. Gómez-Campos, and J. E. Carceller, "Simple analytical valence band structure including warping and non-parabolicity to investigate hole transport in Si and Ge," *Semicond. Sci. Technol.*, vol. 20, no. 1, pp. 16–22, Jan. 2005.
[40] J. B. Arthur, A. C. Baynham, W. Fawcett, and E. G. S. Paige, "Optical absorption due to free holes in germanium: A comparison of theory and experiment," *Phys. Rev.*, vol. 152, no. 2, pp. 740–745, Dec. 1966.
[41] S. K. Ray *et al.,* "Characteristics of THz waves and carrier scattering in boron-doped epitaxial Si and $Si_{1-x}Ge_x$ films," *J. Appl. Phys.*, vol. 95, no. 10, pp. 5301–5304, May 2004.
[42] A. G. U. Perera, W. Z. Shen, W. C. Mallard, M. O. Tanner, and K. L. Wang, "Far-infrared free-hole absorption in epitaxial silicon films for homojunction detectors," *Appl. Phys. Lett.*, vol. 71, no. 4, pp. 515–517, Jul. 1997.
[43] "*MATLAB R2014a*," MathWorks, Natick, MA, USA, 2014.
[44] R. A. Soref and L. Friedman, "Electrooptical modulation in $Si_{1-x}Ge_x$ Si and related heterostructures," *Int. J. Optoelectron.*, vol. 9, no. 2, pp. 205–210, 1994.
[45] P. Moontragoon, R. A. Soref, and Z. Ikonic, "The direct and indirect bandgaps of unstrained $Si_xGe_{1-x-y}Sn_y$ and their photonic device applications," *J. Appl. Phys.*, vol. 112, no. 7, Oct. 2012, Art. ID. 073106.
[46] R. Soref, "Silicon-based silicon–germanium–tin heterostructure photonics," *Philosoph. Trans. A Math. Phys. Eng. Sci.*, vol. 372, no. 2012, Feb. 2014, Art. ID. 20130113.
[47] X. Yang, F. Cheng, and R. Soref, "Single-mode GeSn mid-infrared waveguides on group-IV substrates," in *Proc. CLEO*, San Jose, CA, USA, 2014, pp. 1–2.
[48] R. Soref, J. Hendrickson, and J. W. Cleary, "Mid- to long-wavelength infrared plasmonic-photonics using heavily doped n-Ge/Ge and n-GeSn/GeSn heterostructures," *Opt. Exp.*, vol. 20, no. 4, pp. 3814–3824, Feb. 2012.